Journal of Physics and Chemistry of Solids 78 (2015) 35–40

Contents lists available at ScienceDirect

Journal of Physics and Chemistry of Solids

journal homepage: www.elsevier.com/locate/jpcs

Direct sunlight responsive Ag–ZnO heterostructure photocatalyst: Enhanced degradation of rhodamine B

Hongju Zhai [a], Lijing Wang [a], Dewu Sun [a], Donglai Han [c,d], Bing Qi [a], Xiuyan Li [b], Limin Chang [a,*], Jinghai Yang [b,c]

[a] Key Laboratory of Preparation and Applications of Environmental Friendly Materials of the Ministry of Education, Jilin Normal University, Siping136000, Jilin Province, PR China
[b] Key Laboratory of Functional Materials Physics and Chemistry of the Ministry of Education, Jilin Normal University, Siping 136000, Jilin Province, PR China
[c] Changchun Institute of Optics, Fine Mechanics and Physics, Chinese Academy of Sciences, Changchun 130033, PR China
[d] University of Chinese Academy of Sciences, Beijing 100049, PR China

ARTICLE INFO

Article history:
Received 22 May 2014
Received in revised form
22 October 2014
Accepted 5 November 2014
Available online 8 November 2014

Keywords:
Nanostructures
Semiconductors
Chemical synthesis
X-ray diffraction
Microstructure

ABSTRACT

The catalytic activity of Ag–ZnO heterostructure on the photocatalytic degradation of rhodamine B was investigated. It demonstrated that Ag–ZnO heterostructure exhibited an enhanced photocatalytic activity compared to pure ZnO nanoparticles under direct sunlight. The possible factors to the photocatalytic acitivity of the sample were explored, including Ag content, dispersity and calcination temperature. It was shown that the sample dispersed by PVP, with 5% mol ratio Ag content, calcined at 400 °C showed the highest photocatalytic acitivity and this catalyst was reusable.

1. Introduction

In the past few years, more and more interests have been attracted to the photocatalyst for organic pollutants degradation [1–5], because of its advantages over the traditional techniques, including rapid oxidation rate and without polycyclic products. Among the various photocatalysts, nanostructured ZnO has become a promising photocatalyst and has been widely used due to its strong oxidizing power, non-toxic nature, and low cost [6–10]. Despite its great potential, the photocatalytic efficiency remains very low because of the fast recombination of the photogenerated electron–hole pairs. Furthermore, owing to the special properties of nanomaterials, such as high activity, Van der Waals' forces and high surface energy, nanocatalyst usually become unstable and easily combined together, which may weaken its catalytic activity [11]. To solve this problem, many researches have been done [12,13]. It has been found that the photocatalytic activities of ZnO can be improved by constructing noble metal–ZnO heterostructure, which can increase the rate of electron-transfer process [14–16]. Besides, the heterostructures can fix the metal particles separately to inhibit the aggregation of metal particles, which in turn influences its photocatalytic activity [17–19]. However, to the best of our knowledge, though the synthesis of noble metal–ZnO heterostructures have been studied for several times, including hydrothermal method [20], sol–gel method [21], situ reduction [22], homogeneous precipitation method [23], photodeposition method [24], seed-mediated method [14], liquid deposition [25], glucose-mediated solution-solid route, [26] RF magnetron sputtering [27], etc. But they often need complicated and strict process conditions [28–30]. And little research has focused on investigation the influence factors to the catalytic activities. It is urgent to explore simple preparation and high efficiency of noble metal–ZnO heterostructure and investigate the influence factors to catalyst.

Accordingly, in this paper, the Ag–ZnO heterostructure was obtained and it showed enhanced photocatalytic degradation of rhodamine B (RhB) dye compared to ZnO under direct sunlight. The effect factors to photo catalysis degradation of RhB were investigated systematically. Furthermore, the catalyst can be reused at least four cycles.

* Corresponding author. Fax: +86 4343294566.
E-mail address: changlimin2139@163.com (L. Chang).

http://dx.doi.org/10.1016/j.jpcs.2014.11.004
0022-3697/

2. Experimental

2.1. Materials

All the chemicals used in the experiments were in analytical grade(purchased from Shanghai Chemical Industrial Company) and without further purification, including zinc acetate dihydrate ($Zn(CH_3COO)_2 \bullet 2H_2O$), silver nitrate ($AgNO_3$), PVP(M.w.=20,000), ethanol and rhodamine B (RhB). Deionized water was from analytical laboratory.

2.2. Preparation of Ag–ZnO heterostructure

Ag–ZnO heterostructure was prepared via a simple solvothermal process [31]. For a typical process: to begin with, 1.9 mmol zinc acetate dihydrate and 0.1 mmol silver nitrate were dissolved in ethanol and stired for 30 min. Afterwards, the mixture was added into a teflon-lined stainless steel autoclave (25 mL) and heated at 100 °C for 24 h followed by gradually cooling to room temperature. After being washed by ethanol several times and dried at 80 °C under air atmosphere, the uncalcined 5% mol radio Ag–ZnO heterostructure without PVP was finally obtained. Other control experiments were conducted using the same procedure. The sample of different Ag content were prepared with appropriate ratio of $AgNO_3$ and $Zn(CH_3COO)_2 \bullet 2H_2O$, Ag–ZnO–PVP was prepared except the adding of PVP.

2.3. Sample characterizations

Transmission electron microscopy (JEM-2100 F, JEOL Inc, Japan) was used to investigate the structure and composition of the Ag–ZnO heterostructure. The powder X-ray diffraction (XRD) patterns of the samples were recorded by a Rigaku DMAX2500 X-ray diffractometer using Cu Kα radiation (λ=0.154 nm) at a scanning rate of 5°/min for 2θ ranging from 20° to 80°. UV–vis absorption spectra were taken with a TU-1901 spectrophotometer.

2.4. Procedure for evaluation of photocatalytic activity

The photocatalytic activity of the prepared samples was evaluated by measuring the degradation rate of RhB at ambient temperature in sunny days. The degradation experiments were conducted under direct sunlight. All dye solutions were prepared by deionized water at pH 7. Firstly, 0.01 g of the as-prepared powder sample (ZnO) was dispersed in 10 mL RhB solution with a concentration of 1×10^{-5} mol/L, and then the suspensions was stirred for about 20 min in the dark before irradiation in order to achieve the maximum adsorption of catalyst to the dye, subsequently, the suspension was irradiated under sunlight. Finally, 2 mL $NaBH_4$(1 g/L) was added into the solution, and in a fixed time intervals, the samples were collected in order to track the degradation of RhB until the dye was completely degraded. The catalytic activity of the catalyst heterostructure was calculated according to the decreasing rate of the maximum absorption of RhB (550 nm) wavelength, other control experiments were conducted using the same procedure. Afterwards, the sample with the highest catalytic activity was withdrawn and centrifuged (5000 r/min) for 3 min to separate the catalyst and explore whether it could be reused. In the experiment, 0.04 g of the sample was divided into four equal parts, and added into RhB solution respectively, recording the average degradation rate of the samples. Afterwards, the catalyst was centrifugated, washed and dried at 80 °C, repeating the above experiment four times, make sure each experiment was conducted with the same amount of the catalyst (0.01 g) under same conditions.

3. Results and discussion

3.1. Structure characterizations

The typical TEM images of the obtained Ag–ZnO (5% mol ratio) heterostructure were conducted in order to discuss its microstructures and morphologies. Fig. 1(a) presented a low-magnified TEM image of the sample, whose nanocrystals were of a hexagonal crystalline structure. All of these Ag–ZnO heterostructures closely adhere to each other. Meantime, a high-magnified TEM picture of an individual Ag–ZnO heterostructure was shown in Fig. 1(b), which displayed that Ag core was coated by ZnO shells. The lattice fringe with interplanar spacing of 0.221 nm was corresponding to the (101) plane of ZnO. This close interconnection between Ag cores and ZnO shells was believed to favor the transfer and separation of photo-generated electrons from ZnO shells to the silver cores [32–34], which in turn affected its photocatalytic activity.

XRD patterns of the obtained samples were shown in Fig. 2(a–d). In Fig. 2(a), all the diffraction peaks of wurtzite ZnO were detected without any other impurity peaks, indicating excellent crystal properties and extremely high purity. Meanwhile, the diffraction patterns of heterostructures with different Ag content were shown in Fig. 2(b–d). In Fig. 2(b), two new peaks appeared at 38.8° and 44.2° were corresponding to Ag nanoparticles. However, owing to the fairly low concentration of Ag, its peaks were not obvious and could not be completely detected [35]. When Ag content was increased to 10%, another new peak at 63° appeared in Fig. 2(c–d), and its intensity increased with the increasing of Ag content. All these pattens demonstrated that Ag was successfully combined with ZnO nanoparticles, which was in accordance with the TEM results.

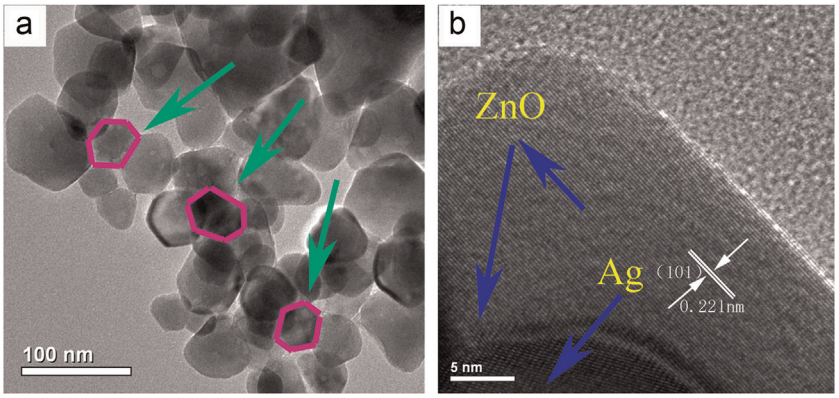

Fig. 1. TEM images of as-prepared Ag–ZnO heterostructure with 5% Ag content.

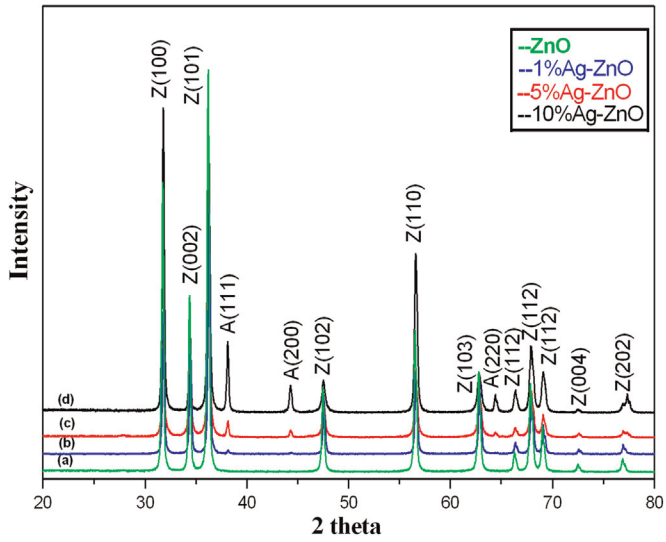

Fig. 2. XRD patterns of as-prepared samples with different Ag content (A for Ag and Z for ZnO).

3.2. Photocatalytic activity

3.2.1. Investigation of degradation of RhB

The time-dependent UV–visible spectra of the mixture of RhB and Ag–ZnO heterostructure were revealed in Fig. 3. The experimental result suggested that the characteristic absorption of RhB at 550 nm decreased gradually, and finally disappeared within 30 min with Ag–ZnO heterostructure (Fig. 3(a)), which displayed higher catalytic efficiency compared to the results of previous studies [11]. While in the control experiment without catalyst (Fig. 3(b)), the degradation of RhB could not be throughly finished in two days. The results exhibited excellent photocatalytic effect of Ag–ZnO heterostructure.

3.2.2. Factors to the photocatalytic activity

In order to explore the optimum value of the photocatalytic activity, factors of Ag content, dispersity and calcination temperature were selected in the experiment. Firstly, catalysts with different Ag content were obtained by adjusting the adding ratio of silver nitrate, the specific data were shown in Table 1, in the expected product, x mol ratio means the content of Ag, and the corresponding photocatalytic activities were shown in Fig. 4, which clearly indicated that the pure ZnO nanocatalyst exhibited photocatalytic activity to a certain extent, however, Ag–ZnO heterostructure showed an enhanced activity compared to pure ZnO. With a low content of Ag, its photocatalytic activity increased with

Table 1
The adding radio of $AgNO_3$ and $Zn(CH_3COO)_2$ in different Ag content catalyst and their corresponding degradation rate of RhB.

Sample	ZnO	1%Ag–ZnO	3%Ag–ZnO	5%Ag–ZnO	7%Ag–ZnO	10%Ag–ZnO
$AgNO_3$: $Zn(CH_3COO)_2$	0	1:99	3:97	5:95	7:93	10:90
Degradation rate (30 min)	35%	65%	82%	90%	80%	75%

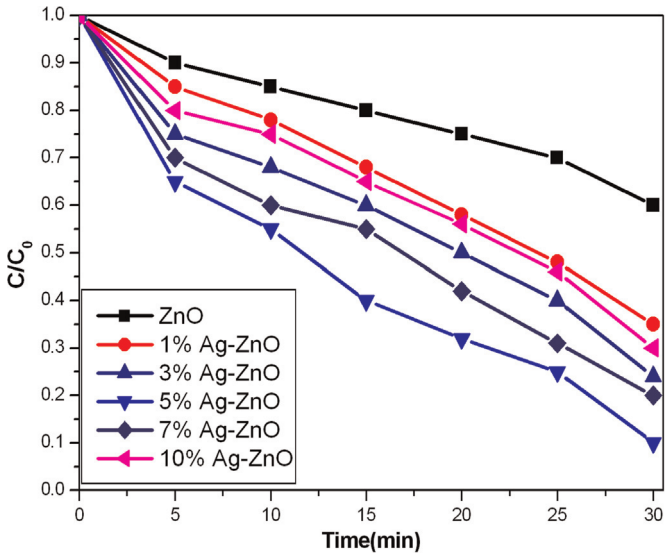

Fig. 4. Degradation of RhB by the as-prepared Ag–ZnO heterostructure with different Ag content.

the increasing of Ag content from 1–5% mol ratio. However, a further increase to 10% led to a reduction of the photocatalytic activity. Thus the optimal Ag content was 5%, and its corresponding apparent rate constant (k) was $3.0\times10^{-2}\,\mathrm{min}^{-1}$ based on $C_0/C=kt$, a value larger than bare ZnO ($1.2\times10^{-2}\,\mathrm{min}^{-1}$) by a factor of 2.5. Meanwhile, as for the results above, possible reasons had been concluded as follows, the degradation of RhB was conducted by the absorption of sunlight photons with an equal or higher energy than the band-gap in ZnO, which led to the formation of photogenerated holes in its valence band (VB) as well as the electrons in its conduction band (CB). Afterwards, CB electrons of ZnO flowed into Ag nanoparticles through the Schottky barrier due to the higher CB level of ZnO compared to Ag nanoparticles. This electron transfer process shared a higher speed than the electron–hole recombination between VB and CB of ZnO [36].

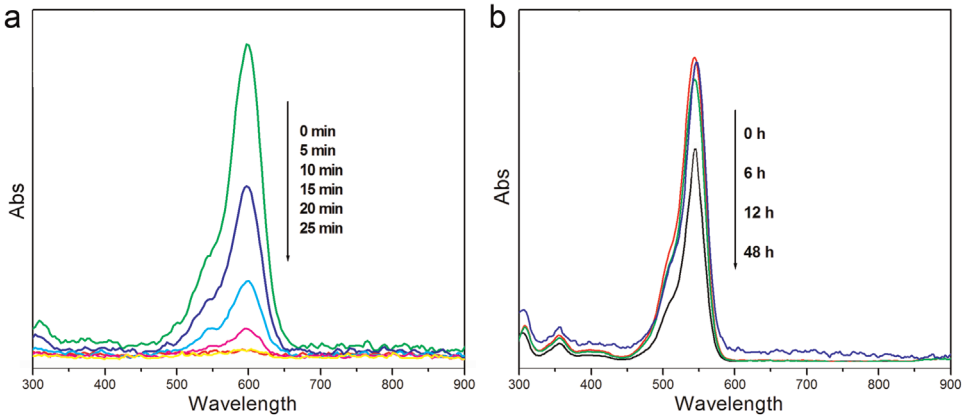

Fig. 3. Time-dependent UV–visible spectra of RhB ethanol solution as function of reaction time with 5% Ag–ZnO as catalyst (a) and pure RhB ethanol solution (b).

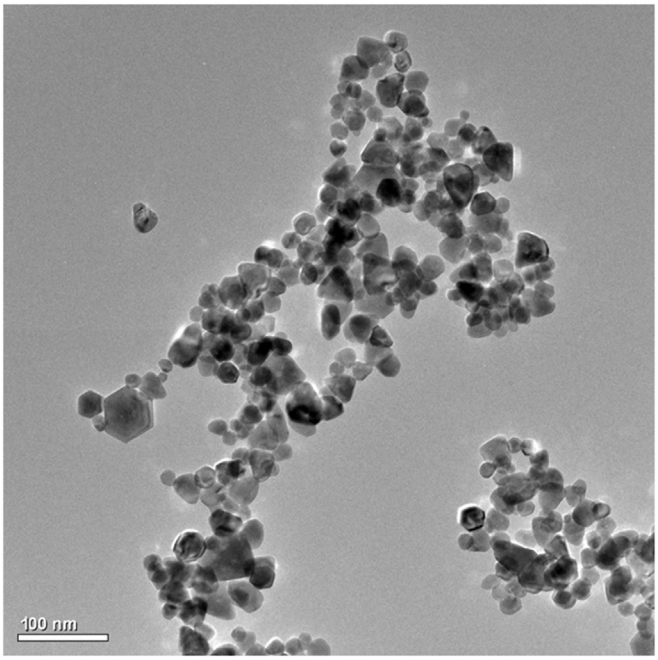

Fig. 5. TEM image of as-prepared Ag–ZnO–PVP heterostructure.

Therefore, lots of CB electrons of ZnO were kept in Ag nanoparticles to decrease the absorption of oxygen effectively [27]. Meanwhile, increasing VB-holes of ZnO with a strong oxidation power escaped from the pair recombination, which was available to oxidize RhB. As a result, Ag–ZnO heterostructure revealed enhanced photocatalytic activity with appropriate Ag content. However, once the combining amount of Ag exceeded a thresholds value, Ag may become the recombination center of photo-generated electrons and holes, it is not conducive to electron–hole separation, which in turn decreased its catalytic activity.

To further explore the effect of particles dispersion to the catalyst, 10 mL PVP with the concentration of 1 g/L was added to the solution during the synthesis process and the Ag–ZnO–PVP was then obtained. The TEM image was shown in Fig. 5, which presented higher dispersity than Ag–ZnO. Afterwards, in the degradation experiment, same amount (0.01 g) of Ag–ZnO and Ag–ZnO–PVP with different Ag content were acted as catalyst

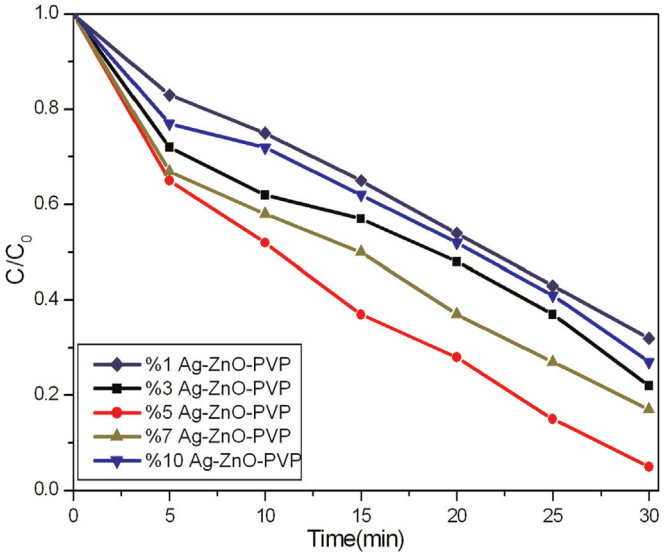

Fig. 6. Degradation rate of RhB of Ag–ZnO–PVP with different Ag contents.

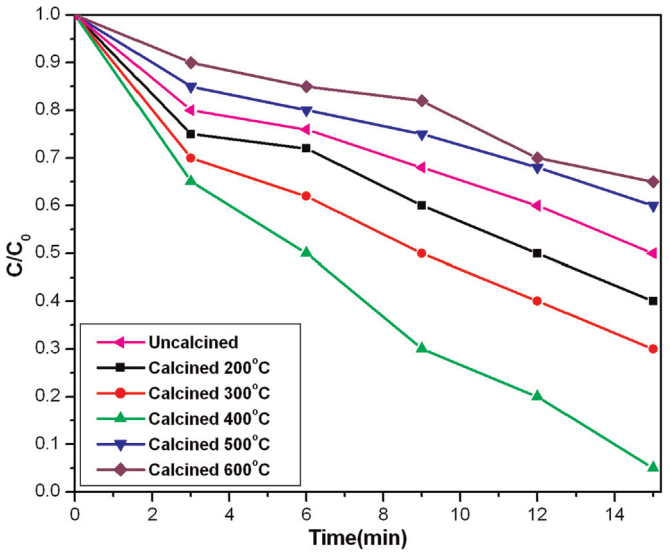

Fig. 7. Degradation rate of RhB by the as-prepared Ag–ZnO heterostructure under different calcination temperature.

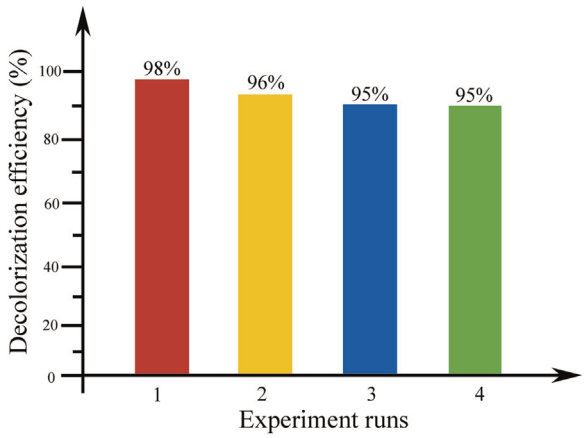

Fig. 8. Degradation rate of RhB for four successive cycles by the as-prepared Ag–ZnO heterostructure.

respectively to degrade RhB and the corresponding spectra was shown in Fig. 6. It is found that the sample with PVP shows better degradation rate compared to the former one. It is related to the enhancement of dispersion of Ag core particle. Once PVP is added to Ag–ZnO core–shell structure, the dispersion of Ag core particle would be enhanced, leading to the further separation and transfer of photoinduced electrons, which increased its degradation rate.

Meanwhile, the sample with different calcination temperature were obtained, during the experiment, the uncalcined sample was equally divided into six portions, and calcined with different temperatures with the same muffle furnace for 2 h, after generally cooling to room temperature, the samples were then taken to explore the catalytic activity and their corresponding degradation rate were shown in Fig. 7. At the very beginning, the photocatalytic activity of the samples were increased with the increasing of calcination temperature, and exhibited the highest activity at calcination temperature of 400 °C. However, the further increase of temperature led to the decrease of degradation efficiency gradually, because with low temperature, zinc acetate can't be completely decomposed, it is not helpful to the formation of ZnO and can hinder the separation of electrons and holes, thus affecting the photocatalytic activity. The higher temperature resulted in the continuous improvement of the crystallinity of ZnO, which

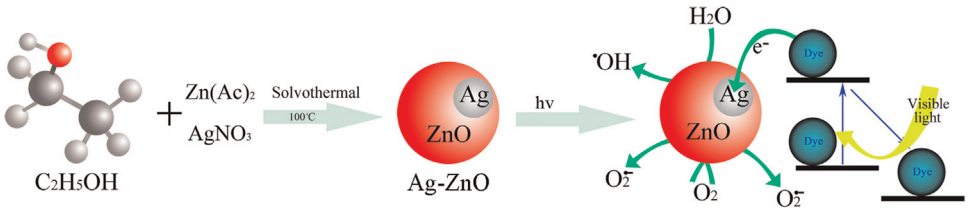

Fig. 9. Mechanism for the fabrication of Ag–ZnO heterostructure and degradation procedure of RhB.

weakened the ability of catalyst in the separation of holes and electrons, which in turn reduced the activity of the photocatalyst.

3.2.3. Photostability of Ag–ZnO heterostructure

The stability of catalyst is an important factor of the catalyst performance, which is tightly related to the cost of the sample, so Ag–ZnO heterostructure was reused to test its stability. The results showed that the photocatalytic activity of Ag–ZnO had little change after each cycle and the corresponding image was shown in Fig. 8. The degradation efficiency for the four cycling reuse were 98%, 96%, 95% and 95% in 30 min respectively, which in turn certificated that our catalyst was stable and shared high photostability under sunlight.

3.3. Mechanism

Based on the above investigations, the mechanisms of the generation and photocatalytic reaction for Ag–ZnO photocatalyst were brought forward, as was presented in Fig. 9. Ag–ZnO heterostructure was prepared by a one-step process in which the $Zn(CH_3COO)_2{\bullet}2H_2O$ and $AgNO_3$ were gradually added into ethanol. After $Zn(CH_3COO)_2{\bullet}2H_2O$ was dissolved, the compound was broken down to generate ZnO nanoparticles at 100 °C (1). Then, the reduction of Ag should also occur during the process of solvothermal treatment (2)–(3). The catalytic process can be explained by an electrochemical mechanism, where silver nanoparticles in Ag–ZnO heterostructure served as an electron relay for an oxidant and a reductant [37,38], and electron transfer occured via the supported Ag particles (4)–(6). Thus it would inhibit the combination of electron–hole pairs to enhance its catalysis activity. The possible reaction formulas for the formation of Ag–ZnO heterostructure and catalysis process were proposed as:

$$Zn(CH_3COO)_2{\bullet}2H_2O \rightarrow ZnO\downarrow + 2CH_3COOH + H_2O \quad (1)$$

$$2CH_2CH_3OH + O_2 \rightarrow 2CH_3CHO + 2H_2O \quad (2)$$

$$CH_3CHO + 2AgNO_3 + H_2O \rightarrow 2Ag\downarrow + 2HNO_3 + CH_3COOH \quad (3)$$

$$Dye + Ag\text{-}ZnO \rightarrow dye^{+\bullet}\ Ag\text{-}ZnO + e^- \quad (4)$$

$$e^- + O_2 \rightarrow O_2^{\bullet -} \quad (5)$$

$$Dye^{+\bullet} + O_2/O_2^{\bullet -} \rightarrow \text{degradation products} \quad (6)$$

4. Conclusions

Well-dispersed Ag–ZnO heterostructure has been successfully prepared by a simple solvothermal process. The photocatalytic activities of ZnO could be further enhanced by the combination with silver nanoparticles. When Ag loading was 5% mol ratio with the adding of PVP and calcination temperature of 400 °C, the sample revealed the highest photocatalytic acitivity and the catalyst was reusable. The Ag–ZnO heterostructure would show promising application in the degradation of organic dyes in the industry owing to its advantage of simplicity, low consumption, and excellent performance.

Acknowledgments

This work is supported by National Programs for High Technology Research and Development of China (863) (Item no. 2013AA032202), the National Natural Science Foundation of China (Grant nos. 61308095 and 61378085), Program for the development of Science and Technology of Jilin province (Item no. 20130102004JC, 20140101160JC), the Program for the Innovation of Youth Talents of Jilin Normal University (Item no. JSDCXRC2011-13), the Program for the masters scientific and innovative research of Jilin Normal University (Item no. 2013027).

References

[1] K.Q. Zhou, Q.J. Zhang, Y.Q. Shi, S.H. Jiang, Y. Hu, G. Zhou, J. Alloys Compd. 577 (2013) 389–394.
[2] J.C. Li, Y.F. Li, T. Yang, B. Yao, Z.H. Ding, Y. Xu, Z.Z. Zhang, L.G. Zhang, H.F. Zhao, D.Z. Shen, J. Alloys Compd. 550 (2013) 479–482.
[3] S.K. Kansal, M. Singh, D. Sud, J. Hazard Mater. 141 (2007) 581–590.
[4] A. Bianco-Prevot, A. Basso, C. Baiocchi, M. Pazzi, G. Marci, V. Augugliaro, L. Palmisano, E. Pramauro, Anal. Bioanal. Chem. 378 (2004) 214–220.
[5] W.I. Nawawi, M.A. Nawi, J. Mol. Catal. A Chem. 383 (2014) 83–93.
[6] Y. Li, B.P. Zhang, J.X. Zhao, J. Alloys Compd. 586 (2014) 663–668.
[7] S. Kumar, P. Kaur, C.L. Chen, R. Thangavel, C.L. Dong, Y.K. Ho, J.F. Lee, T.S. Chan, T.K. Chen, B.H. Mok, S.M. Rao, ., J. Alloys Compd. 588 (2014) 705–709.
[8] Y. Xi, W.Z. Wu, H. Fang, C.G. Hu, J. Alloys Compd. 529 (2012) 163–168.
[9] C.H. Xia, F. Wang, C.L. Hu, J. Alloys Compd. 589 (2014) 604–608.
[10] S. Sönmezoğlu, V. Eski Zeybek, A. Toumiat, A. Avcı, J. Alloys Compd. 586 (2014) 593–599.
[11] C.X. Song, Y.S. Lin, D.B. Wang, Z.S. Hua, Mater. Lett. 64 (2010) 1595–1597.
[12] Y. Du, R.Z. Chen, J.F. Yao, H.T. Wang, J. Alloys Compd. 551 (2013) 125–130.
[13] X.Z. Li, Y.Q. Wang, J. Alloys Compd. 509 (2011) 5765–5768.
[14] X.T. Yin, W.X. Que, D. Fei, F.Y. Shen, Q.S. Guo, J. Alloys Compd. 524 (2012) 13–21.
[15] Y.G. Xu, H. Xu, J. Yan, H.M. Li, L.Y. Huang, J.X. Xia, S. Yin, H.M. Shu, Colloid Surf. A 436 (2013) 474–483.
[16] L.H. Xu, G. Zheng, M. Lai, S. Pei, J. Alloys Compd. 583 (2014) 560–565.
[17] H.R. Liu, G.X. Shao, J.F. Zhao, Z.X. Zhang, Y. Zhang, J. Liang, X.G. Liu, H.S. Jia, B.S. Xu, J. Phys. Chem. C 116 (2012) 16182–16190.
[18] Q. Zhang, C.G. Tian, A.P. Wu, Y. Hong, M.X. Li, H.G. Fu, J. Alloys Compd. 563 (2013) 269–273.
[19] B. Subash, B. Krishnakumar, M. Swaminathan, M. Shanthi, Mater. Chem. Phys. 141 (2013) 114–120.
[20] S.Y. Gao, Y. Ji, X.X. Jia, S.X. Yang, Z.D. Li, K. Jiang, J. Solid State Chem. 184 (2011) 764–769.
[21] C. Karunakaran, V. Rajeswari, P. Gomathisankar, Mater. Sci. Semicond. Process. 14 (2011) 133–138.
[22] P. Zhang, C.L. Shao, X.H. Li, X. Zhang, Y.Y. Sun, Y.C. Liu, J. Hazard Mater. 237-238 (2012) 331–338.
[23] Z.G. Jia, K.K. Peng, Y.Y. Li, R.S. Zhu, Trans. Nonferr. Met. Soc. China 22 (2012) 873–878.
[24] J. Wang, X.M. Fan, K. Tian, Z.W. Zhou, Y. Wang, Appl. Surf. Sci. 275 (2011) 7763–7770.
[25] Z.J. Li, S.Y. Sun, X. Xu, B. Zheng, A. Meng, Catal. Commun. 12 (2011) 890–894.
[26] C.G. Tian, Q. Zhang, B.J. Jiang, G.H. Tian, H.G. Fu, J. Alloys Compd. 509 (2011) 6935–6941.
[27] T. Tian, Y. Li, B. Wang, X.M. Song, E. Li, H. Wang, H. Yan, Mater. Chem. Phys. 111 (2008) 305–308.
[28] E.F. Keskinler, M. Tomakin, S. Doğan, G. Turgut, S. Aydın, S. Duman, B. Gürbulak, J. Alloys Compd. 550 (2013) 129–132.

[29] B. Subash, B. Krishnakumar, M. Swaminathan, M. Shanthi, Langmuir 29 (2013) 939–949.
[30] Z.Z. Han, L.L. Ren, Z.H. Cui, C.Q. Chen, H.B. Pan, J.Z. Chen, Appl. Catal. B Environ. 126 (2012) 298–305.
[31] H.J. Zhai, L.J. Wang, D.L. Han, H. Wang, J. Wang, X.Y. Liu, X. Lin, X.Y. Li, M. Gao, J.H. Yang, J. Alloys Compd. 600 (2014) 146–150.
[32] B. Subash, B. Krishnakumar, B. Sreedhar, M. Swaminathan, M. Shanthi, Superlattice Microsoft 54 (2013) 155–171.
[33] S.I. Inamdar, K.Y. Rajpure, J. Alloys Compd. 595 (2014) 55–59.
[34] D.H. Yoo, T.V. Cuong, V.H. Luan, N.T. Khoa, E.J. Kim, S.H. Hur, S.H. Hahn, J. Phys. Chem. C 116 (2012) 7180–7184.
[35] Y.H. Li, J. Gong, G.H. He, Y.L. Deng, Mater. Chem. Phys. 134 (2012) 1172–1178.
[36] L. Han, D.J. Wang, Y.C. Lu, T.F. Jiang, L.P. Chen, T.F. Xie, Y.H. Lin, Sens. Actuators B Chem. 177 (2013) 34–40.
[37] K.J. Liu, J.Y. Zhang, H. Gao, T.F. Xie, D.J. Wang, J. Alloys Compd. 552 (2013) 299–303.
[38] L. Shi, L. Liang, J. Ma, Y.N. Meng, S.F. Zhong, F.X. Wang, J.M. Sun., Ceram. Int. 40 (2014) 3495–3502.